Inorganic Chemistry

Article

pubs.acs.org/IC

Effects of Solvation on the Framework of a Breathing Copper MOF Employing a Semirigid Linker

Christopher R. Murdock, Zheng Lu, and David M. Jenkins*

Department of Chemistry, The University of Tennessee, Knoxville, Tennessee, 37996-1600, United States

Supporting Information

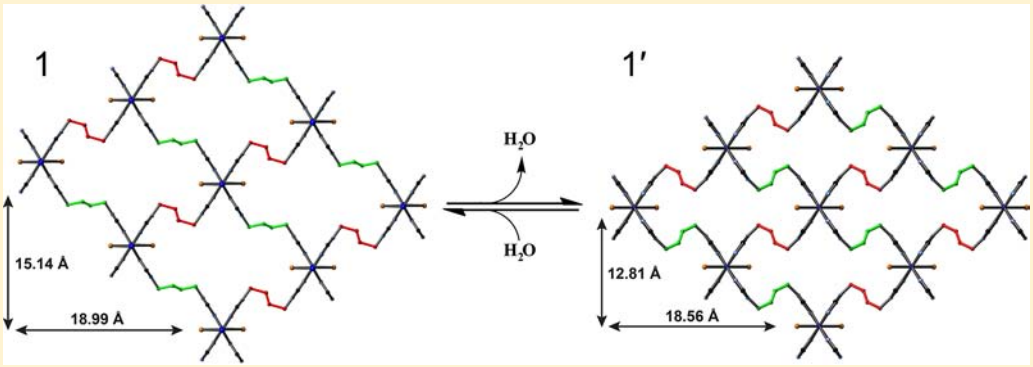

ABSTRACT: A semirigid di-1,2,4-triazole ligand leads to formation of the MOF $[Cu_2(\mathbf{L})_2(SO_4)(Br)_2]\cdot xH_2O$ (**1**). The framework structure of **1** flexes reversibly upon removal or addition of water to form semihydrated ($[Cu_2(\mathbf{L})_2(SO_4)(Br)_2]\cdot 4H_2O$) and dehydrated ($[Cu_2(\mathbf{L})_2(SO_4)(Br)_2]\cdot 0H_2O$) MOFs, **1′** and **1″**, respectively. Single-crystal X-ray analysis demonstrated that the 2-butene subunit of the ligand rotates between two positions for **1** and **1′**, causing a change in the solvent-accessible volume in the framework. This double hinge within the semirigid ligand is a built-in breathing mechanism and suggests a novel approach for general synthesis of breathing MOFs.

INTRODUCTION

Due to their potential importance in applications such as gas separations,[1] liquid separations,[2] chemical sensing,[3] and even drug delivery,[4] breathing MOFs (metal−organic frameworks) have become an important class of multifunctional porous materials. Breathing MOFs undergo a reversible expansion and contraction of the void space in the framework due to the presence or absence of guest molecules.[5] A simple flexing of the framework to accommodate its guest frequently leads to highly selective guest adsorption.[3b,4a,5c] For example, selective gas adsorption has been demonstrated for separations of CO_2 versus CH_4,[1a−d,3a] N_2,[1a,d,f,h,3a] and H_2.[1d−f] Given their ability to exhibit high guest selectivity and the challenge for their preparation, synthetic methodologies for rational synthesis of breathing MOFs are sorely desired.[5]

Myriad strategies have been pursued to synthesize 3D breathing materials that change their void space as a function of guest.[5] Kitagawa describes three classes of 3D breathing materials: 2D coordination polymer layers that are connected by a flexible ligand in the third dimension (Class a), 1D coordination polymer chains that form a rhombus (or certain other geometric shapes) in the other two dimensions (Class b), and 3D interpenetrated grids (Class c) (Figure 1).[5b] The breathing MOFs from Class a have demonstrated large breathing behavior with a range of flexible linkers between their 2D polymeric layers.[6] However, synthesis of additional MOFs of this type is challenging because it remains a struggle to control the number of linkers between each 2D layer.[6a,b] In a similar manner, while interpenetrated grids have shown phase

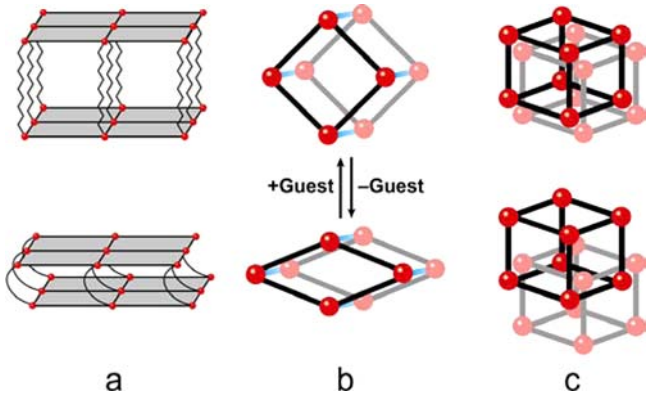

Figure 1. Illustration of three classes of 3D breathing materials. All materials are shown expanded on top and contracted on bottom. (a) 2D coordination polymer layers that are connected by a flexible ligand in the third dimension; (b) 1D coordination polymer chains (blue lines) that form a rhombus in the other two dimensions; (c) 3D interpenetrated grids.

Received: November 30, 2012
Published: February 5, 2013

   dx.doi.org/10.1021/ic3026304 | *Inorg. Chem.* 2013, 52, 2182−2187

transitions upon solvation/desolvation, which can selectively trap CO_2 in the nanopores at low pressures,[1d] it is quite challenging to rationally synthesize new variants on this class of MOF because the degree of interpenetration is not predictable.[7] Since the SBUs (secondary building units) of Class b materials are similar to many MOFs that have previously been prepared,[8] this class of breathing MOFs has attracted the most attention.[9]

Férey and Serre prepared a series of Class b breathing MOFs.[9a−f] The critical feature is a ditopic carboxylate attached to an inorganic brick (SBU) that has a mirror plane. The breathing mechanism is activated by rotation around the O−O axis of the carboxylate (known as the "kneecap"), which requires an opposite rotation on the opposing side of the SBU.[5c,9e] While Férey and Serre effectively described this mechanism and identified examples of this class of breathing MOFs, preparing additional MOFs of this type has been challenging, in part because the inorganic bricks that fit their requirements are quite rare.[5c,10]

More recently, Long and co-workers reported two other Class b breathing MOFs that utilized 1,4-benzene-di(1*H*-1,2,3-triazole)[1g] or 1,4-benzenedipyrazolate[11] as the bridging ligand instead of a ditopic carboxylate. In the triazole system, the flexing was caused by two separate bending points: a small one within the ligand and the larger one at the metal−ligand interface. For the pyrazolate-based cobalt MOF, the structure undergoes a complex five-step transition that involves a rearrangement at the cobalt center wherein the geometry about the metal ion shifts from square planar to tetrahedral. Notably, the "kneecap", the primary flexing point, in both of their systems is still located at the junction of the ligand and metal.[1g,11]

A problem with expanding Class b breathing MOFs is that they all depend on the exact interaction of the binding angle between the ligand and the metal. Our objective is to move the "kneecap" from the metal−ligand junction to within the ligand itself. We are developing MOFs utilizing semirigid ligands that have two points of rotation between the ditopic binding to the rigid metal−ligand fragment. These double hinges effectively make the ligand act like a "screw", which twists so that the angles of the rhombus shift without any significant effects at the metal−ligand binding points. The elegance of this method is that the degree of breathing can be incorporated by judicious choice of semirigid ligands that conform to this double-hinged design motif.

In this article, we describe the synthesis and characterization of a copper MOF with a semirigid linker that displays reversible structural changes due to solvation/desolvation in the framework. Crucially, single-crystal characterization shows these structural changes are the result of the rotation of a subunit of the ligand and not a change in the metal−ligand bond, which ultimately affects the void volume of the framework but not the topology. This change in void volume is demonstrated via gas adsorption experiments with an increase in adsorption for both CO_2 and CH_4 as a function of increased water in the pores.

EXPERIMENTAL SECTION

The compound 4,4′-(1,4-(*trans*-2-butene)diyl)bis(1,2,4-triazole) (notated below as "**L**") was prepared as described previously.[12] All other reagents were purchased from commercial vendors and used without purification. Infrared spectra were collected on a Thermo Scientific Nicolet iS10 with a Smart iTR accessory for attenuated total reflectance. Thermogravimetric analysis (TGA) data were collected on a TA Instruments TGA Q50 under N_2. Carbon, hydrogen, and nitrogen analyses were obtained from Atlantic Microlab, Norcross, GA. Single-crystal diffraction data was collected on a Bruker SMART APEX II three-circle diffractometer equipped with a CCD area detector and operated at 1800 W power (45 kV, 40 mA) to generate Mo Kα radiation (λ = 0.71073 Å). The incident X-ray beam was focused and monochromated using Bruker Excalibur focusing optics. Single crystals of **1** and **1′** were mounted on nylon CryoLoops (Hampton Research) with Paratone-N (Hampton Research) and frozen at −100 and −173 °C, respectively. The sulfate anions in both cases are heavily disordered. Due to the large void volume, water molecules were not located. In both cases, SQUEEZE routine was used to simplify and improve the refinements. Additionally, all structures were examined using the *Addsym* subroutine of PLATON[13] to ensure that no additional symmetry could be applied to the models. Powder X-ray diffraction (PXRD) data was collected using a Panalytical Empyrean θ−2θ diffractometer in reflectance Bragg−Brentano geometry. Cu Kα radiation (λ = 1.5406 Å; 1800 W, 45 kV, 40 mA) was focused using a planar Gobel Mirror riding the Kα line. Gas adsorption measurements were collected at 298 K on a Micromeritics ASAP 2020.

Synthesis of $[Cu_2(L)_2(SO_4)(Br)_2]\cdot xH_2O$, 1. Copper(II) sulfate pentahydrate (9.18 mg, 0.0367 mmol) and a mixture of potassium bromide (8.75 mg, 0.0735 mmol) and **L** (14.0 mg, 0.0735 mmol) were added to separate 4 mL scintillation vials and dissolved with 1 and 2 mL of water, respectively. The vials were heated to 85 °C for 30 min in an aluminum heating block. Solutions were mixed and heated for an additional 1 h until large blue crystalline needles formed. Crystalline material was collected from the mother liquor and washed with H_2O to remove excess ligand. IR (neat): 3349, 3135, 1640, 1561, 1497, 1444, 1401, 1377, 1360, 1280, 1216, 1088, 1066, 1046, 972, 944, 880, 742, 680 cm^{-1}. Crystal data for **1** $C_{16}H_{20}Br_2Cu_2N_{12}O_4S$, M = 763.40, triclinic, space group $P\bar{1}$, a = 7.260(16) Å, b = 11.77(3) Å, c = 13.15(3) Å, α = 74.55(3)°, β = 76.47(3)°, γ = 76.55(3)°. V = 1036(4) Å^3, Z = 1, ρ_{calcd} = 1.224 Mg m^{-3}, μ(Mo Kα) = 3.036 mm^{-1}; 7844 collected reflections, 2839 crystallographically independent reflections [R_{int} = 0.1421], θ_{max} = 23.34°, goodness-of-fit =1.028. R_1 = 0.1711, wR_2 = 0.3766 [$I > 2\sum(I)$]; R_1 = 0.2125, wR_2 = 0.4152 (all data).

Synthesis of $[Cu_2(L)_2(SO_4)(Br)_2]\cdot 4H_2O$, 1′. Air drying **1** for 15 min resulted in formation of the partially dehydrated framework, **1′**, and remained as blue crystalline needles (5.6 mg, 37% yield; yield was based on starting copper sulfate). IR (neat): 3362, 3138, 2964, 1636, 1560, 1496, 1444, 1401, 1377, 1361, 1279, 1261, 1214, 1089, 1064, 1046, 974, 948, 879, 797, 742, 680 cm^{-1}. Anal. Calcd for $C_{16}H_{20}Br_2Cu_2N_{12}O_4S\cdot 4H_2O$: C, 23.00; H, 3.38; N, 20.12. Found: C, 22.54; H, 3.75; N, 18.63. Crystal data for **1′**: $C_{16}H_{20}Br_2Cu_2N_{12}O_4S$, M = 763.40, monoclinic, space group $C2/c$, a = 12.813(6) Å, b = 18.557(8) Å, c = 7.259(3) Å, β = 111.973(5)°. V = 1600.7(12) Å^3, Z = 2, ρ_{calcd} = 1.584 Mg m^{-3}, μ(Mo Kα) = 3.930 mm^{-1}; 2919 collected reflections, 622 crystallographically independent reflections [R_{int} = 0.0912], θ_{max} = 18.75°, goodness-of-fit = 1.465. R_1 = 0.1148, wR_2 = 0.3305 [$I > 2\sum(I)$]; R_1 = 0.1366, wR_2 = 0.3534 (all data).

Synthesis of $[Cu_2(L)_2(SO_4)(Br)_2]\cdot 0H_2O$, 1. A sample of **1′** was heated to 100 °C in a 20 mL scintillation vial in an aluminum heating block. A green powder, **1″**, was formed after 1 h of heating. Anal. Calcd for $C_{16}H_{20}Br_2Cu_2N_{12}O_4S$: C, 25.17; H, 2.64; N, 22.02. Found: C, 24.43; H, 2.90; N, 20.97.

Time-Dependent Reactions for Desolvation/Resolvation of 1. **1** was synthesized according to the above method, and an immediate PXRD was taken of the as synthesized crystals. PXRD patterns were then taken at 5, 10, and 15 min to monitor the dehydration process. Upon desolvation, the powder was resolvated by adding 5 drops of H_2O and gently soaking up any excess solvent. A PXRD pattern was then taken at 15 min to show the desolvated phase, and this process was repeated again as can be seen in Figure 3.

TGA Measurements. Thermogravimetric analysis (TGA) data were collected on a TA Instruments TGA Q50 under N_2. All TGAs were collected at a ramp rate of 5 °C/min under N_2 atmosphere. TGA of **1** was obtained by soaking a sample of **1′** in water for 1 h. PXRD was taken of a small sample of the material to ensure the sample was in

dx.doi.org/10.1021/ic3026304 | *Inorg. Chem.* 2013, 52, 2182−2187

the correct phase as **1**. Upon removal from solution, excess water was collected using filter paper and TGA was immediately collected. TGA of **1′** was obtained after placing a sample in a desiccator for 24 h using the same initial sample as **1**.

Gas Adsorption Measurements. Gas adsorption measurements were collected at 298 K on a Micromeritics ASAP 2020. Gas adsorption measurements were performed on a fresh sample of **1′**, which was verified by PXRD. The sample was first degassed at 100 °C for 1 h to form the completely dehydrated framework **1″**, and CO_2 and CH_4 measurements were collected at 298 K. After data collection, 2 mL of H_2O was added to the sample and allowed to soak for 1 h. After soaking, the sample was collected and washed with acetone and placed in a desiccator for 24 h. PXRD was taken to verify the sample was in the **1′** phase prior to CO_2 and CH_4 measurements.

RESULTS AND DISCUSSION

We previously reported the synthesis of the semirigid di-1,2,4-triazole, 4,4′-(1,4-(*trans*-2-butene)diyl)bis(1,2,4-triazole), denoted as **L**.[12] Adding 2 equiv of both **L** and potassium bromide to copper sulfate yields $[Cu_2(\mathbf{L})_2(SO_4)(Br)_2]\cdot xH_2O$ (**1**) as blue needle-shaped crystals after 1 h at 85 °C (Scheme 1, Reaction

Scheme 1. Synthesis of Copper MOFs Designated 1, 1′, and 1″

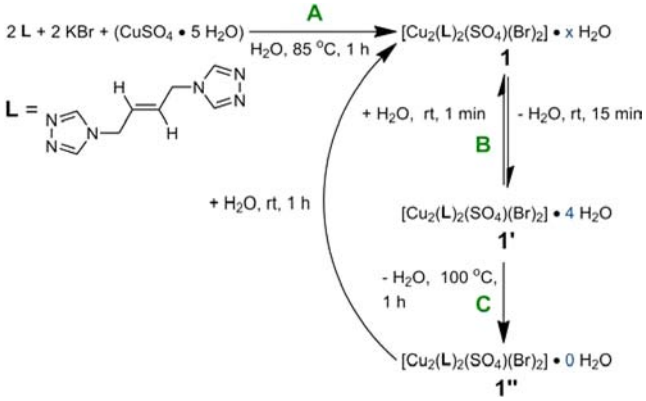

A). Single-crystal X-ray studies of the blue needles revealed that compound **1** crystallizes in the $P\bar{1}$ space group. Each octahedral copper center is coordinated by four triazole ligands that form an equatorial plane and two bromides in the axial positions. Adjacent copper atoms along the *x* axis are bridged by two triazole fragments using the two terminal nitrogen atoms on each triazole and a bridging bromide to form a linear chain (Figure 2a). These chains are linked in the other two dimensions by the second triazole moiety of the ligand, forming the three-dimensional network, while the sulfates remain in the pores (Figure 2b).

While the PXRD of a fresh sample of **1** matches its simulated powder pattern, a considerable shift in the PXRD pattern can be seen in aged samples. Our suspicion for the cause of the shift in the PXRD was a loss of the guest molecules from within the pores. To confirm our suspicion, a time-dependent PXRD of **1** was performed and revealed that the pattern of **1** was changed to the semihydrated form (**1′**) within 15 min, and the pattern of **1′** is stable for days (Figure 3). Additionally, **1′** will fully revert to **1** upon resolvation when a few drops of water are added onto the sample. This reversible process could be repeated multiple times without apparent crystallinity change.

To determine the extent of hydration in **1** and **1′** we conducted TGA measurements. The amount of lattice water that resides in **1** cannot be determined from TGA measure-

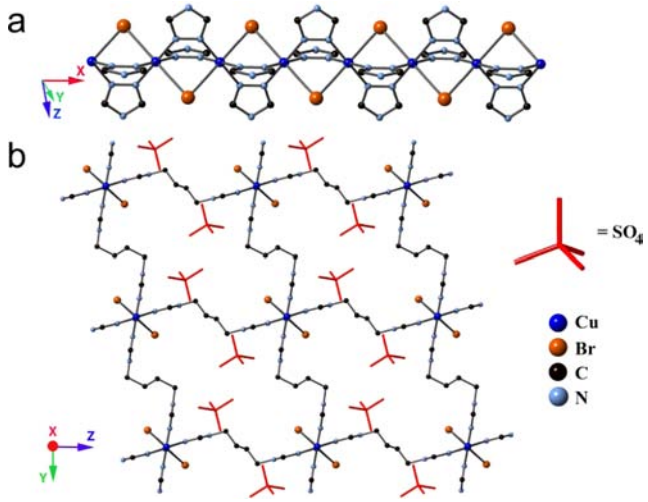

Figure 2. (a) Crystal structure of **1** showing copper chains formed along the *x* axis. (b) Crystal structure of **1** showing links between copper chains viewed orthogonal to the *x* axis.

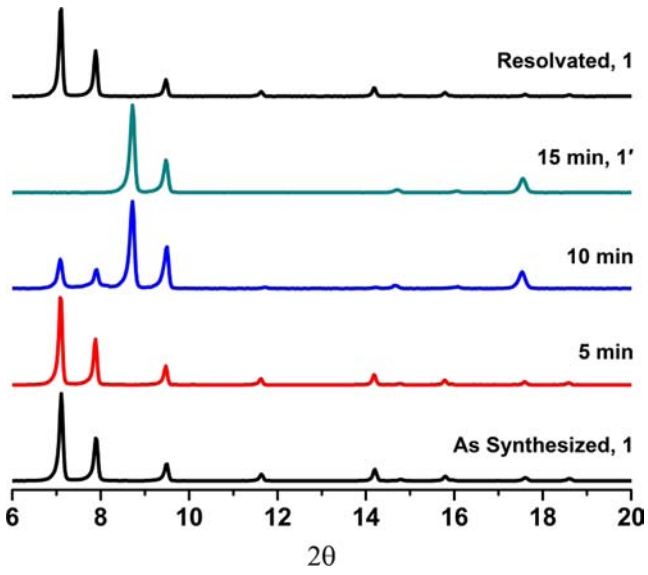

Figure 3. Powder pattern X-ray diffraction measurements taken of samples of the desolvation of **1** to **1′** and back to **1**. **1′** is fully formed from **1** within 15 min. **1** can be reformed by resolvating the sample of **1′**. Intensity was normalized for each pattern.

ments since MOF **1** loses the excess water very quickly at room temperature to give **1′**. Immediate removal of **1** from a water bath results in a TGA trace shown in Figure 4. The initial weight loss can be attributed primarily to surface water.[14] MOF **1′**, on the other hand, loses 8.9% of its mass at 86 °C, which is consistent with four water molecules in the pores (Figure 4). From the weight loss, we can deduce the formula for **1′** is $[Cu_2(\mathbf{L})_2(SO_4)(Br)_2]\cdot 4H_2O$ (Scheme 1). Notably, the TGA trace for **1** shows additional weight loss at the same temperature, leading us to conclude that by 86 °C we already formed **1′**.

To further understand this reversible process, single-crystal X-ray diffraction was performed on a carefully air-dried single crystal of **1**. Air-dried **1** (compound **1′**) maintains the macroscopic morphology of blue needles, but the space group changes to *C*2/*c*. The X-ray crystal structure demonstrated that the topologies of **1** and **1′** are the same

dx.doi.org/10.1021/ic3026304 | *Inorg. Chem.* 2013, 52, 2182−2187

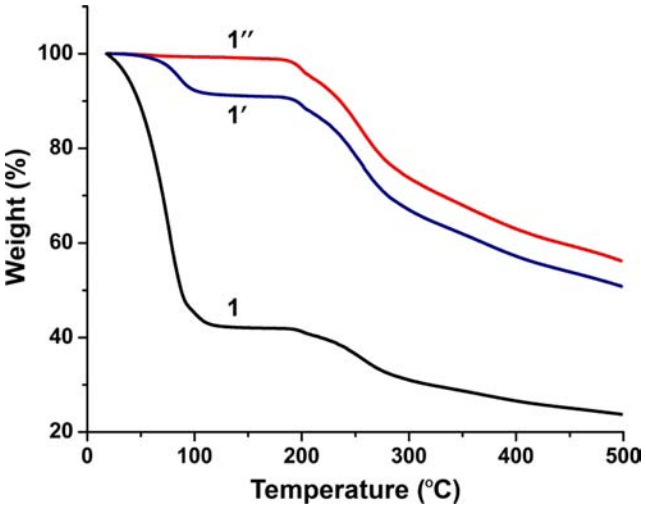

Figure 4. TGA measurements for **1**, **1′**, and **1″**.

and that there was no appreciable change along the vector containing the Cu−Br bonds (Figure 1 and Supporting Information Figure S1).

Despite having the same topologies, several structural differences between **1** and **1′** are observed. A significant change in the axis lengths on the rhombus perpendicular to the 1D coordination polymer chains is detected with the vertical height decreasing by over 2.3 Å (Figure 5a and 5b). Furthermore, in contrast to Long's system, a small decrease in axial length of 0.4 Å was also noted.[1g] These changes to the size of the pore channels lead to a 29% increase in density between **1** (1.224 g/cm^3) and **1′** (1.584 g/cm^3). Although the solvent molecules within the framework were not located due to poor crystallinity, the solvent-accessible volume in each framework was calculated using PLATON.[13] The solvent-accessible volume of **1** is 21% larger than **1′** (35.6% for **1** versus 14.8% for **1′**).

To understand what causes these structural differences between **1** and **1′** we evaluated the positions of the bridging ligand, **L**, in relation to the 1D chain composed of Cu and Br atoms. MOF **1** has two crystallographically distinct bridging 1,2,4-ditriazoles (Figure 5a, shown in red and green highlights). The 2-butene portion of **L** highlighted in green in Figure 5a is pointed almost orthogonal to the *yz* plane. The dihedral angle between the two planes composed of the 1D coordination polymer chain (the Cu and Br atoms) and the 2-butene portion of **L** is 33°. The second distinct bridging **L** highlighted in red in Figure 5a has a dihedral angle of 82° between the 1D coordination polymer chain and the 2-butene.

In MOF **1′**, one of the 2-butene subunits of the bridging ligand **L** has rotated to become the mirror image of the other one, and they are no longer crystallographically distinct (Figure 5b). The 2-butene portion highlighted in red has barely shifted and has a dihedral angle of 83° with respect to the Cu and Br atoms, but the other 2-butene fragment, highlighted in green, has rotated substantially, now showing a dihedral angle of 97° (Figure 5b). This twisting about one pair of 2-butene subunits on the opposite edges of the rhombus causes the Cu−Br layers to pack more tightly (Figure 5c and 5d), demonstrating that in this system the orientation of the 2-butene subunit acts as the "kneecap". To the best of our knowledge, this result is the first case where the "kneecap" is entirely based in the ligand and not primarily at the metal−ligand junction.

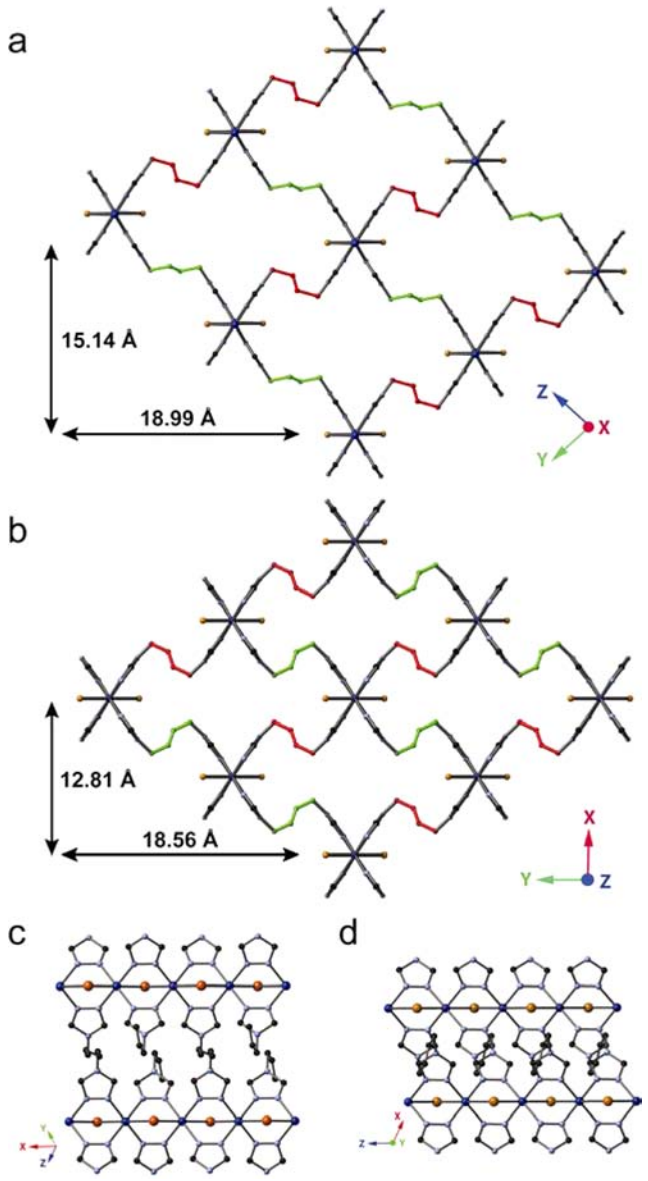

Figure 5. (a and b) Distances shown are rhombus axes. Red and green highlights are 2-butene subunits of ligand that correspond to same position in **1** and **1′**. (a) Crystal structure of **1** viewed orthogonal to the *x* axis. (b) Crystal structure of **1′** viewed orthogonal to the *z* axis. (c) Crystal structure of **1** viewed along the *x* axis. (d) Crystal structure of **1′** viewed along the *z* axis. In all structures, sulfates have been omitted for clarity.

TGA measurements show that **1′** is only partially dehydrated (Figure 4), suggesting that it may be possible to give a fully desolvated MOF. If the remaining guest molecules could be removed, the 2-butene subunits may rotate to a different position, which may further decrease the void volume. To investigate the effect of further dehydration on the flexibility of the framework, a fully dehydrated MOF was prepared. A sample of **1′** was heated to 100 °C for 1 h. A green powder corresponding to $[Cu_2(\mathbf{L})_2(SO_4)(Br)_2]\cdot 0H_2O$ (**1″**) was obtained. TGA was taken of **1″**, and there was no weight loss until the framework itself decomposed, providing evidence the framework had been completely desolvated (Figure 4). Due to the poor crystallinity of **1″**, we were not able to obtain a single crystal. However, a PXRD pattern of **1″** shows that although the material is almost amorphous, one peak persists

dx.doi.org/10.1021/ic3026304 | *Inorg. Chem.* 2013, 52, 2182−2187

after heating, which is at $2\theta = 9.4°$. This peak is also present in the PXRD patterns of both **1** and **1′** (Figure 3). Indexing of the PXRD patterns of **1** and **1′** indicates that this peak represents their (011) and (020) planes, respectively (see Supporting Information Figures S2a and S2b). The similarity of these two planes is most clearly seen along the copper−bromide vectors in **1** and **1′** (Figure 5c and Figure 5d). Conceivably, this same ordered plane exists in the fully dehydrated **1″**, while randomly oriented ethylene chains cause disorder, leading to a mostly amorphous state. Finally, if a sample of **1″** is left in water for 1 h, adsorption of water allows for reformation of blue **1** based on PXRD measurements. Attempts at forming **1** from **1″** through the use of water vapor were unsuccessful, and it was determined that only liquid water allowed for successful reformation of **1**. The newly reformed **1** can then be cycled through **1′** and subsequently **1″**.

The presence of guest molecules within a framework, specifically polar guests such as water, has recently been shown to improve CO_2 adsorption or selectivity.[15] This increase in adsorption by polar guests can be attributed to the significant quadrupole moment of CO_2 which favors interactions such as hydrogen bonding with the guest molecules.[1b,15a,c−e] On the other hand, adsorption of gases, such as CH_4 that exhibit no quadrupole moment, is not favored in the presence of polar guests.[1b,15a,c] The flexibility exhibited by this MOF system as well as the presence of water as a guest molecule piqued our interest in studying their CO_2 adsorption properties and, in particular, their selectivity for CO_2 versus nonpolar guests, such as CH_4, as a function of guest water molecules. Since no crystal structure could be obtained for **1″**, adsorption isotherms may also provide evidence for expansion in the solvent-accessible volume of **1′** versus **1″**.

Due to the rapid dehydration of **1** to **1′**, adsorption properties of the fully hydrated **1** were not able to be analyzed; however, adsorption isotherms could be performed and compared between the fully dehydrated **1″** and the partially dehydrated **1′**. Figure 6 shows both the CO_2 and the CH_4 adsorption isotherms for **1′** and **1″** at 298 K. At 1.22 bar, the CO_2 and CH_4 uptakes for **1″** are 0.490 and 0.0285 mmol g^{-1}, respectively. When the framework is expanded to **1′** after careful hydration treatment, the adsorption isotherms drastically change. An increase in adsorption is witnessed, resulting in the uptake of 1.39 mmol g^{-1} of CO_2 and 0.160 mmol g^{-1} of CH_4 at 1.22 bar. Since both CO_2 and CH_4 adsorption increased, the selectivity did not appear to change significantly even though polar guests are present within the framework.

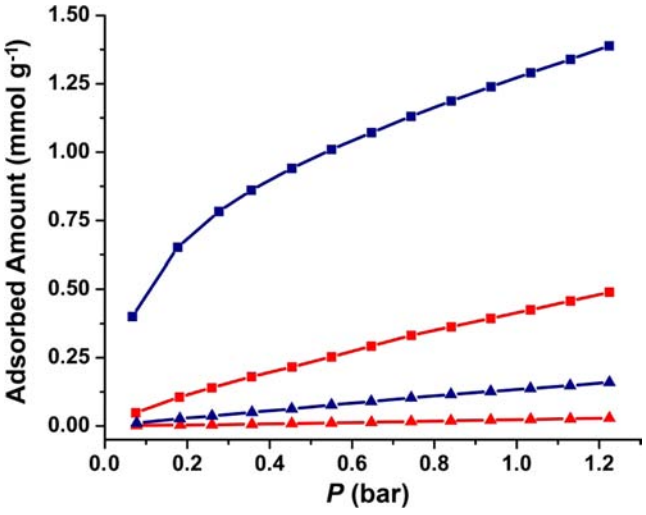

Figure 6. CO_2 (squares) and CH_4 (triangles) depict adsorption isotherms for **1′** (blue) and **1″** (red) at 298 K.

As mentioned above, polar guests, such as water, have been demonstrated to improve the CO_2/CH_4 selectivity due to the different interactions between the guest molecules and adsorbent. By analyzing the isotherms and the transition from **1″** to **1′**, the adsorption behavior experienced does not follow the normal trend and, instead, the adsorption of water and expansion of the framework allows for an increase in both CO_2 and CH_4 adsorption for **1′** when compared to **1″**. In other systems, the presence of water has been shown to decrease CH_4 adsorption, therefore increasing selectivity for CO_2.[1b,15a,c] A plausible explanation for the increase in adsorption for both CO_2 and CH_4 in **1′** is the expansion of the framework in addition to any interactions with the guest water molecules present.

CONCLUSION

A three-dimensional copper MOF was synthesized that changes its framework structure as a function of the quantity of interstitial water molecules. The orientation of the semirigid di-1,2,4-triazole ligand adjusts as a function of hydration, and this process is reversible at room temperature. Furthermore, the MOF loses much of its crystallinity when the remaining water molecules are removed (as seen in **1″**), but **1** can be recovered in its powder form by addition of water. Single-crystal X-ray diffraction demonstrates that this breathing MOF constructed with semirigid linkers has the ability to self-adjust the solvent-accessible volume according to the amount of solvent present while maintaining the same topology. Notably, the "kneecap" in this breathing system lies within the ligand itself and not at the metal−ligand juncture. The quantity of gases adsorbed increased for both CO_2 and CH_4 with a structural change that was facilitated by addition of guest water molecules. Finally, the selectivity of CO_2 versus CH_4 adsorption is not increased with water in the pores, which is contrary to what is typically observed for MOFs that have been partially hydrated. Since similar semirigid linkers are easy to synthesize and their flexibility can be modulated, this strategy could lead to a large family of porous materials that change their void space as a function of guest adsorption.

ASSOCIATED CONTENT

Supporting Information

X-ray crystallographic data (CIF) and diagrams of single-crystal data for **1′** and PXRD data for **1** and **1′**. This material is available free of charge via the Internet at http://pubs.acs.org.

AUTHOR INFORMATION

Corresponding Author

*E-mail: Jenkins@ion.chem.utk.edu.

Notes

The authors declare no competing financial interest.

ACKNOWLEDGMENTS

We are grateful to the state of Tennessee's Science Alliance whose JDRD grant provided partial support for this research.

REFERENCES

(1) (a) Kitaura, R.; Seki, K.; Akiyama, G.; Kitagawa, S. *Angew. Chem., Int. Ed.* **2003**, *42*, 428. (b) Llewellyn, P. L.; Bourrelly, S.; Serre, C.; Filinchuk, Y.; Férey, G. *Angew. Chem., Int. Ed.* **2006**, *45*, 7751. (c) Chen, B.; Ma, S.; Zapata, F.; Fronczek, F. R.; Lobkovsky, E. B.; Zhou, H.-C. *Inorg. Chem.* **2007**, *46*, 1233. (d) Yang, S.; Lin, X.; Lewis, W.; Suyetin, M.; Bichoutskaia, E.; Parker, J. E.; Tang, C. C.; Allan, D. R.; Rizkallah, P. J.; Hubberstey, P.; Champness, N. R.; Thomas, K. M.; Blake, A. J.; Schroeder, M. *Nat. Mater.* **2012**, *11*, 710. (e) Chen, B.; Liang, C.; Yang, J.; Contreras, D. S.; Clancy, Y. L.; Lobkovsky, E. B.; Yaghi, O. M.; Dai, S. *Angew. Chem., Int. Ed.* **2006**, *45*, 1390. (f) Thallapally, P. K.; Tian, J.; Kishan, M. R.; Fernandez, C. A.; Dalgarno, S. J.; McGrail, P. B.; Warren, J. E.; Atwood, J. L. *J. Am. Chem. Soc.* **2008**, *130*, 16842. (g) Demessence, A.; Long, J. R. *Chem.—Eur. J.* **2010**, *16*, 5902. (h) Li, J.-R.; Ma, Y.-G.; McCarthy, M. C.; Sculley, J.; Yu, J.-M.; Jeong, H.-K.; Balbuena, P. B.; Zhou, H.-C. *Coord. Chem. Rev.* **2011**, *255*, 1791. (i) Wuttke, S.; Bazin, P.; Vimont, A.; Serre, C.; Seo, Y.-K.; Hwang, Y. K.; Chang, J.-S.; Férey, G.; Daturi, M. *Chem.—Eur. J.* **2012**, *18*, 11959. (j) Xiang, S.; He, Y.; Zhang, Z.; Wu, H.; Zhou, W.; Krishna, R.; Chen, B. *Nat. Commun.* **2012**, *3*, 954. (k) Han, S.; Huang, Y.; Watanabe, T.; Dai, Y.; Walton, K. S.; Nair, S.; Sholl, D. S.; Meredith, J. C. *ACS Comb. Sci.* **2012**, *14*, 263.

(2) (a) El Osta, R.; Carlin-Sinclair, A.; Guillou, N.; Walton, R. I.; Vermoortele, F.; Maes, M.; de Vos, D.; Millange, F. *Chem. Mater.* **2012**, *24*, 2781. (b) Dan-Hardi, M.; Chevreau, H.; Devic, T.; Horcajada, P.; Maurin, G.; Férey, G.; Popov, D.; Riekel, C.; Wuttke, S.; Lavalley, J.-C.; Vimont, A.; Boudewijns, T.; de Vos, D.; Serre, C. *Chem. Mater.* **2012**, *24*, 2486.

(3) (a) Henke, S.; Schneemann, A.; Wuetscher, A.; Fischer, R. A. *J. Am. Chem. Soc.* **2012**, *134*, 9464. (b) Dybtsev, D. N.; Chun, H.; Kim, K. *Angew. Chem., Int. Ed.* **2004**, *43*, 5033.

(4) (a) Horcajada, P.; Serre, C.; Maurin, G.; Ramsahye, N. A.; Balas, F.; Vallet-Regi, M.; Sebban, M.; Taulelle, F.; Férey, G. *J. Am. Chem. Soc.* **2008**, *130*, 6774. (b) Della Rocca, J.; Liu, D.; Lin, W. *Acc. Chem. Res.* **2011**, *44*, 957. (c) Taylor-Pashow, K. M. L.; Della Rocca, J.; Xie, Z.; Tran, S.; Lin, W. *J. Am. Chem. Soc.* **2009**, *131*, 14261. (d) Huxford, R. C.; Della Rocca, J.; Lin, W. *Curr. Opin. Chem. Biol.* **2010**, *14*, 262.

(5) (a) Kitagawa, S.; Kitaura, R.; Noro, S.-i. *Angew. Chem., Int. Ed.* **2004**, *43*, 2334. (b) Uemura, K.; Matsuda, R.; Kitagawa, S. *J. Solid State Chem.* **2005**, *178*, 2420. (c) Férey, G.; Serre, C. *Chem. Soc. Rev.* **2009**, *38*, 1380.

(6) (a) Alberti, G.; Giontella, E.; Murcia-Mascarós, S. *Inorg. Chem.* **1997**, *36*, 2844. (b) Alberti, G.; Murcia-Mascarós, S.; Vivani, R. *J. Am. Chem. Soc.* **1998**, *120*, 9291. (c) Kitaura, R.; Fujimoto, K.; Noro, S.-i.; Kondo, M.; Kitagawa, S. *Angew. Chem., Int. Ed.* **2002**, *41*, 133.

(7) (a) Chen, B.; Ma, S.; Zapata, F.; Lobkovsky, E. B.; Yang, J. *Inorg. Chem.* **2006**, *45*, 5718. (b) Uribe-Romo, F. J.; Hunt, J. R.; Furukawa, H.; Kloeck, C.; O'Keeffe, M.; Yaghi, O. M. *J. Am. Chem. Soc.* **2009**, *131*, 4570.

(8) Férey, G.; Mellot-Draznieks, C.; Serre, C.; Millange, F.; Dutour, J.; Surble, S.; Margiolaki, I. *Science* **2005**, *309*, 2040.

(9) (a) Serre, C.; Millange, F.; Thouvenot, C.; Nogues, M.; Marsolier, G.; Loueer, D.; Férey, G. *J. Am. Chem. Soc.* **2002**, *124*, 13519. (b) Loiseau, T.; Serre, C.; Huguenard, C.; Fink, G.; Taulelle, F.; Henry, M.; Bataille, T.; Férey, G. *Chem.—Eur. J.* **2004**, *10*, 1373. (c) Serre, C.; Millange, F.; Surble, S.; Férey, G. *Angew. Chem., Int. Ed.* **2004**, *43*, 6286. (d) Surble, S.; Serre, C.; Mellot-Draznieks, C.; Millange, F.; Férey, G. *Chem. Commun.* **2006**, 284. (e) Serre, C.; Mellot-Draznieks, C.; Surble, S.; Audebrand, N.; Filinchuk, Y.; Férey, G. *Science* **2007**, *315*, 1828. (f) Horcajada, P.; Salles, F.; Wuttke, S.; Devic, T.; Heurtaux, D.; Maurin, G.; Vimont, A.; Daturi, M.; David, O.; Magnier, E.; Stock, N.; Filinchuk, Y.; Popov, D.; Riekel, C.; Férey, G.; Serre, C. *J. Am. Chem. Soc.* **2011**, *133*, 17839. (g) Serre, C.; Surble, S.; Mellot-Draznieks, C.; Filinchuk, Y.; Férey, G. *Dalton Trans.* **2008**, 5462. (h) Mellot-Draznieks, C.; Serre, C.; Surble, S.; Audebrand, N.; Férey, G. *J. Am. Chem. Soc.* **2005**, *127*, 16273. (i) Alaerts, L.; Maes, M.; Giebeler, L.; Jacobs, P. A.; Martens, J. A.; Denayer, J. F. M.; Kirschhock, C. E. A.; De Vos, D. E. *J. Am. Chem. Soc.* **2008**, *130*, 14170. (j) Finsy, V.; Kirschhock, C. E. A.; Vedts, G.; Maes, M.; Alaerts, L.; De Vos, D. E.; Baron, G. V.; Denayer, J. F. M. *Chem.—Eur. J.* **2009**, *15*, 7724. (k) Couck, S.; Denayer, J. F. M.; Baron, G. V.; Remy, T.; Gascon, J.; Kapteijn, F. *J. Am. Chem. Soc.* **2009**, *131*, 6326. (l) Salles, F.; Bourrelly, S.; Jobic, H.; Devic, T.; Guillerm, V.; Llewellyn, P.; Serre, C.; Férey, G.; Maurin, G. *J. Phys. Chem. C* **2011**, *115*, 10764.

(10) Férey, G. *Dalton Trans.* **2009**, 4400.

(11) (a) Choi, H. J.; Dincă, M.; Long, J. R. *J. Am. Chem. Soc.* **2008**, *130*, 7848. (b) Salles, F.; Maurin, G.; Serre, C.; Llewellyn, P. L.; Knöfel, C.; Choi, H. J.; Filinchuk, Y.; Oliviero, L.; Vimont, A.; Long, J. R.; Férey, G. *J. Am. Chem. Soc.* **2010**, *132*, 13782.

(12) Murdock, C. R.; Lu, Z.; Jenkins, D. M. *Dalton Trans.* **2012**, *41*, 7839.

(13) Spek, A. L. *J. Appl. Crystallogr.* **2003**, *36*, 7.

(14) (a) Yun, S. K.; Pinnavaia, T. J. *Chem. Mater.* **1995**, *7*, 348. (b) Qian, K.; Fang, G.; Wang, S. *Chem. Commun.* **2011**, *47*, 10118. (c) Abid, H. R.; Tian, H.; Ang, H.-M.; Tade, M. O.; Buckley, C. E.; Wang, S. *Chem. Eng. J.* **2012**, *187*, 415.

(15) (a) Yazaydin, A. O.; Benin, A. I.; Faheem, S. A.; Jakubczak, P.; Low, J. J.; Willis, R. R.; Snurr, R. Q. *Chem. Mater.* **2009**, *21*, 1425. (b) Jiang, J. *AIChE J.* **2009**, *55*, 2422. (c) Liu, B.; Smit, B. *J. Phys. Chem. C* **2010**, *114*, 8515. (d) Liu, J.; Wang, Y.; Benin, A. I.; Jakubczak, P.; Willis, R. R.; Le Van, M. D. *Langmuir* **2010**, *26*, 14301. (e) Soubeyrand-Lenoir, E.; Vagner, C.; Yoon, J. W.; Bazin, P.; Ragon, F.; Hwang, Y. K.; Serre, C.; Chang, J.-S.; Llewellyn, P. L. *J. Am. Chem. Soc.* **2012**, *134*, 10174.